Development 133, 2947-2959 (2006) doi:10.1242/dev.02454

Brachyury is required for elongation and vasculogenesis in the murine allantois

Kimberly E. Inman and Karen M. Downs*

Mouse conceptuses homozygous for mutations in brachyury (*T*) exhibit a short, misshapen allantois that fails to fuse with the chorion. Ultimately, mutant embryos die during mid-gestation. In the 60 years since this discovery, the role of *T* in allantoic development has remained obscure. T protein was recently identified in several new sites during mouse gastrulation, including the core of the allantois, where its function is not known. Here, using molecular, genetic and classical techniques of embryology, we have investigated the role of *T* in allantoic development. Conceptuses homozygous for the $T^{Curtailed}$ (T^{C}) mutation (T^{C}/T^{C}) exhibited allantoic dysmorphogenesis shortly after the allantoic bud formed. Diminution in allantoic cell number and proliferation was followed by cell death within the core. Fetal liver kinase (Flk1)-positive angioblasts were significantly decreased in T^{C}/T^{C} allantoises and did not coalesce into endothelial tubules, possibly as a result of the absence of platelet endothelial cell adhesion molecule 1 (Pecam1), whose spatiotemporal relationship to Flk1 suggested a role in patterning the umbilical vasculature. Remarkably, microsurgical perturbation of the wild-type allantoic core phenocopied the T^{C}/T^{C} vascularization defect, providing further support that an intact core is essential for vascularization. Last, abnormalities were observed in the T^{C}/T^{C} heart and yolk sac, recently reported sites of T localization. Our findings reveal that T is required to maintain the allantoic core, which is essential for allantoic elongation and vascular patterning. In addition, morphological defects in other extraembryonic and embryonic vascular organs suggest a global role for *T* in vascularization of the conceptus.

KEY WORDS: Allantois, Anteroposterior axis, Apoptosis, Brachyury, Primitive streak, Patterning, Proliferation, Vasculogenesis, Mouse, Yolk sac, Heart

INTRODUCTION

The evolutionarily conserved T-box family of transcription factors shares a common DNA-binding domain, the T-box. T-box genes exhibit dynamic expression patterns during embryogenesis, and genetic alterations suggest that they play important, although largely unexplained, roles during development (Naiche et al., 2005; Papaioannou, 2001; Showell et al., 2004). The founding member of this family, *T*, was identified in mice as a semi-dominant mutation affecting tail length in heterozygous adults (Dobrovolskaia-Zavadskaia, 1927). *T/T* mutants died during mid-gestation (Chesley, 1935; Zavadskaia and Kobozieff, 1930), presumably because of a failure of the developing umbilicus, the allantois, to unite with the chorion and vascularize it to form a functional chorio-allantoic placenta (Gluecksohn-Schoenheimer, 1944).

The allantois is derived from epiblast, the progenitor tissue of all three primary germ layers (Lawson et al., 1991). Once the primitive streak, or future anteroposterior (AP) axis, appears, proximal epiblast ingresses into the posterior streak and emerges as mesoderm, some of which is displaced into the extraembryonic region to form the allantois. Two morphologically distinct cell types are identifiable in the allantoic bud: an outer layer of squamous epithelial cells, the 'mesothelium' (Downs et al., 2004; Snell and Stevens, 1966); and inner cells, referred to collectively as the 'allantoic core' (Downs and Gardner, 1995).

The allantoic bud then enlarges by cell proliferation, addition of mesoderm from the streak, and distal cavitation (Brown and Papaioannou, 1993; Downs and Bertler, 2000). Allantoic core mesoderm differentiates de novo into the umbilical vasculature by vasculogenesis, as evidenced by the appearance of scattered angioblasts containing Flk1 (Kdr – Mouse Genome Informatics), a tyrosine kinase receptor for vascular endothelial growth factor (Vegf) (Millauer et al., 1993; Yamaguchi et al., 1993), initially in the distal region of the allantois, farthest away from the embryo (Downs et al., 1998). Continued formation of angioblasts and subsequent coalescence into endothelial tubules then follows a spatiotemporally regulated distal-to-proximal sequence such that, by 4- to 6-somite pairs (-s), the nascent Flk1 vascular plexus reaches the base of the allantois and merges with those of the yolk sac and embryo (Downs et al., 1998; Downs et al., 2004). Allantoic vasculogenesis is not accompanied by primitive erythropoiesis; once vascular amalgamation takes place, primitive erythroid cells enter the allantois from the yolk sac (Downs et al., 1998).

The elongated allantois contacts the chorion and fuses with it by 6- to 8-s, in a process that is dependent upon the developmental maturity of the allantois (Downs and Gardner, 1995). Chorio-allantoic union is mediated by chorio-adhesive mesothelial cells, located in the distal allantoic region (Downs and Gardner, 1995) and identified by gradual localization of vascular cell adhesion molecule 1 (Vcam1) (Downs, 2002; Gurtner et al., 1995; Kwee et al., 1995). Recent studies have suggested that differentiation of allantoic mesoderm into its three known cell types, angioblasts/endothelium, mesothelium and chorio-adhesive cells, is intrinsic to the allantois and is not dependent upon the primitive streak; nonetheless, information from the streak consigns the Vcam1 chorio-adhesive cell domain to the distal allantoic region (Downs et al., 2004).

Subsequent to molecular cloning of *T* (Herrmann et al., 1990), expression studies placed *T* within most sites defective in *T/T* mutants, namely the primitive streak and its derivatives, the node, notochord, nascent mesoderm and gut endoderm (Wilkinson et al.,

Department of Anatomy, University of Wisconsin – Madison School of Medicine and Public Health, 1300 University Avenue, Madison, WI 53706, USA.

*Author for correspondence (e-mail: kdowns@wisc.edu)

Accepted 23 May 2005

1990). Results of chimeric studies in *T/T*↔+/+ conceptuses suggested that *T* acted in a cell-autonomous manner within the embryonic body (Rashbass et al., 1991; Wilson et al., 1993). However, discrepancies in *T* expression within the allantois (Herrmann, 1991; Wilkinson et al., 1990), together with inadequate understanding of the fundamental parameters of allantoic development, confounded the interpretation of abnormalities observed within *T/T* chimeric allantoises (Rashbass et al., 1991; Wilson et al., 1993). In light of a recent model of allantoic ontogeny (Downs et al., 2004), we set out to discover the role of *T* in the allantois.

We recently re-investigated the spatiotemporal localization of T within the murine gastrula, employing sectional, rather than whole mount, immunohistochemistry, and paying particular attention to the allantois (Inman and Downs, 2006). In addition to identifying T protein in the heart and a variety of non-mesodermal sites, including extraembryonic and embryonic visceral endoderm and chorionic ectoderm, we localized T to a novel domain, the allantoic core. T was not present in the early allantoic bud (EB). Then, between the neural plate/late allantoic bud (LB) and 6-s stages, a period that coincides with allantoic elongation toward the chorion (~7.5-8.5 dpc), T identified an allantoic core domain that formed an uninterrupted continuum with embryonic T in the primitive streak. By 6- to 8-s, when all normal allantoises have united with the chorion (Downs, 2002; Downs and Gardner, 1995), allantoic T had disappeared, but it persisted in the streak and its anterior derivatives, the node and notochord.

Although the original *T* mutation has most frequently been selected for study, it encompasses a 200 kilobase (kb) deletion (Herrmann et al., 1990) that eliminates at least one other gene, brachyury 2 (*T2*) (Rennebeck et al., 1998; Rennebeck et al., 1995). Thus, to elucidate the role of *T* in the allantois, we selected T^C, a radiation-induced (Searle, 1966) 19 base pair (bp) deletion in exon 8 of *T* that results in a codon frame-shift postulated to produce a C-terminally truncated protein product (Herrmann and Kispert, 1994). Our findings revealed that, in the absence of T, cell proliferation was reduced in the allantois and core cells died, the major consequences of which were foreshortening of the allantois and defective vasculogenesis. As abnormalities were also observed in the heart and yolk sac, both of which were recently identified as novel T sites (Inman and Downs, 2006), our data point not only to a major role for T in formation of the umbilical vasculature, but also to widespread T function in vascularization of the murine conceptus.

MATERIALS AND METHODS

For all experiments, $n \geqslant 3$ specimens for all stages and genotypes presented, unless otherwise noted. All animals were treated in accordance with Public Health Service (PHS) Policy on Humane Care and Use of Laboratory Animals (Public Law 99-158) as enforced by the University of Wisconsin-Madison.

Animal husbandry, intercross mating, dissection, staging and genotyping

Animals were maintained under a 12-hour light/dark cycle (lights out 13:00). T^C/+ breeding couples were established when animals were 3-months old, and were provided with plastic igloos (BioServ, Frenchtown, NJ) to improve nesting and breeding performance. Three lines of T^C mice were generated (Table 1). Expected 1:1 Mendelian ratios were exhibited only in STOCK-T^C/J^{Down} (Table 1); furthermore, offspring exhibited increased fertility and decreased incidence of anal atresia relative to the other two mouse lines (Table 1), and were thus used throughout the study. To obtain T^C/T^C conceptuses, STOCK-T^C/J^{Down} T^C/+ females (3- to 6-months old) were paired with T^C/+ males (3- to 10-months old) prior to the start of the dark cycle. Females were examined for a copulation plug 4 and 15 hours later, and the time of conception was taken as the midpoint of the dark cycle. Pregnant females were killed by CO_2 asphyxiation. Estrus selection, dissection and embryo staging were as previously described (Downs, 2006; Downs and Davies, 1993; Downs and Gardner, 1995). Briefly, stages and their equivalent approximate days post-coitum (dpc) were: early, mid- and late streak (ES, MS, LS) stages, ~6.75-7.0 dpc; early and late allantoic bud (EB, LB) stages, ~7.25-7.5 dpc; and early and late headfold (EHF, LHF) stages, ~7.75-8.0 dpc. Thereafter, staging was by numbers of somite pairs (1- to 2-s, 8.0-8.25 dpc; 2- to 4-s, 8.25 dpc; 4- to 6-s, 8.25-8.5 dpc; 6- to 8-s, 8.5 dpc). Until 4- to 6-s, T^C/T^C conceptuses were staged by development of anterior structures, after which they were assigned the average stage of +/+ and T^C/+ littermates. For genotyping, a small piece of yolk sac or anterior embryonic tissue was taken, after which conceptuses were rinsed in phosphate-buffered saline (PBS, Sigma, St Louis, MO) before processing (below). DNA was extracted in 25 mM NaOH (20 minutes, 95°C), followed by neutralization with 40 mM Tris (pH 5.2), and precipitation using sodium acetate and Pellet Paint (EMD Biosciences, San Diego, CA). The polymerase chain reaction (PCR) protocol used was a modification of that described by Stott et al. (Stott et al., 1993), with primers (5′-TGCAAAGCCCTGTGATGCAA-3′ and 5′-ACATCGGAGAACCAGAAGACGA-3′) that identified a 267-bp T^+ and a 248-bp T^C allele. Reactions were run on a 4% GQA Sieve agarose gel (ISC Bioexpress, Kaysville, UT). By ~9.5 dpc, only one T^C/T^C conceptus was recovered from three litters of timed intercross matings, and none on later days, indicating that T^C/T^C mutants died between ~9.5 and 10.5 dpc (Table 2). For apoptosis pilot experiments and production of 'wild-type' whole and bisected allantoic explants (Fig. 5B, parts g-m), the F2 generation of matings between the inbred hybrid strain B6CBAF1/J (Jackson Laboratories) was used (Downs, 2006). For the Flk1/Pecam allantois whole-mount expression studies (Fig. 6A), a male Kdr^{tm1Jrt} mouse (hereafter referred to as Flk1^{lacZ}) (Shalaby et al., 1995) re-derived on the CD1 background was generously provided by Dr T. N. Sato and mated to females of the inbred hybrid strain B6CBAF1/J; conceptuses were collected between the LB- and 6-s stages.

Histology and sectional immunohistochemistry

Histology and sectional immunohistochemistry were carried out as previously described (Downs, 2002; Downs et al., 2004; Inman and Downs, 2006). Stock concentrations (200 μg/ml) of antibodies (Santa Cruz Biotechnologies, Santa Cruz, CA; T, sc-17743; Vcam1, sc-1504; Flk1, sc-315g; and Bmp4, sc-6896) were used at 1:100, 1:90, 1:50 and 1:90 working dilutions, respectively. For Vcam1, signal was amplified using the Tyramide Signal Amplification (TSA) Kit (Perkin-Elmer, Shelton, CT) according to

Table 1. Fertility and incidence of anal atresia in T^C/+ mice associated with genetic background

Genetic background	Percentage of successful matings*	Total number of litters	Average litter size (average number of litters per pair)	+/+ Offspring (% with anal atresia)	T^C/+ Offspring (% with anal atresia)	*P*-value for χ^2 analyses of Mendelian inheritance
C3.Cg-T^C	48.9	38	6.2 (2.2)	165 (0)	73 (33.0†)	$\leqslant 1\times10^{-13}$
B6.C3(Cg)-T^C	45.8	30	6.6 (2.7)	117 (0)	81 (19.8‡)	$\leqslant 0.001$
STOCK-T^C/J^{Down}	69.2	141	8.1 (3.9)	586 (0)	557 (6.29§)	0.26

The total live-born offspring recovered from T^C/+×+/+ matings was used to determine expected values for χ^2 analyses on each genetic background. For C3H.Cg-T^C, B6.C3(Cg)-T^C and STOCK-T^C/J^{Down}, χ^2=35.56, 6.55 and 0.74, respectively.
*At least 24 breeding pairs of each background were paired continuously for 4 months. Failure to produce a litter within this window was classified as infertile.
†8.33%, ‡75.0% and §28.5% of these also displayed hindlimb defects and a grossly shortened body.

Table 2. Recovery of conceptuses from intercross matings of T^C/+ mice

	Age							
Genotype	~6.75 dpc *n* (%)	~7.5 dpc *n* (%)	~8.0 dpc *n* (%)	~8.5 dpc *n* (%)	~9.0 dpc *n* (%)	~9.5 dpc *n* (%)	~10.5 dpc *n* (%)	~13.5 dpc *n* (%)
+/+	14 (25.0)	31 (22.5)	123 (25.7)	31 (23.8)	7 (31.8)	3 (27.3)	6 (31.6)	4 (20.0)
T^C/+	24 (42.9)	68 (49.3)	234 (49.0)	56 (43.1)	8 (36.4)	7 (63.6)	8 (42.1)	8 (40.0)
T^C/T^C	13 (23.2)	32 (23.2)	96 (20.1)	38 (29.2)	7 (31.8)	1 (9.1)	0	0
Resorptions	5 (8.9)	7 (5.0)	25 (5.2)	5 (3.8)	0	0	5* (26.3)	8† (40.0)
Number of litters	6	17	54	20	3	3	2	2

All genotypes were confirmed by PCR. For all stages the expected percentage of +/+, T^C/+ and T^C/T^C conceptuses was 25%, 50% and 25%, respectively. Where possible (from ~10.5-13.5 dpc), resorbing conceptuses were genotyped. Death of the conceptus was defined as absence of heart beat.
*One T^C/+ conceptus was dead and resorbing; all other dead, resorbing conceptuses were T^C/T^C.
†Two T^C/+ conceptuses were dead and resorbing; all other dead, resorbing conceptuses were T^C/T^C.

the manufacturer's instructions. Detection was with 3,3′-diaminobenzidine (DAB) in chromogen solution (Dako, Carpinteria, CA) and was followed by counterstaining with hematoxylin.

Whole-mount immunostaining for Pecam1

Flk1^{lacZ} conceptuses were fixed in 4% paraformaldehyde (2 hours, 4°C), rinsed in PBS, and then X-gal stained for 2 hours, as previously reported (Downs et al., 2004). Yolk sac, amnion and chorion were dissected away, and specimens were processed and stained according to published methods (Schlaeger et al., 1995) with the following modifications. Blocking solutions contained goat serum (Chemicon), and ready-to-use ABC reagent (Vector Laboratories, Burlingame, CA) was applied prior to the DAB color reaction. Primary antibody was monoclonal rat anti-mouse Pecam1 (Mec13.3) diluted 1:100 (537355, BD Biosciences, San Jose, CA). Secondary antibody was a biotinylated goat anti-rat IgG diluted 1:500 (sc-2041, Santa Cruz Biotechnologies). Conceptuses were developed for 5 minutes at room temperature after which they were re-fixed in paraformaldehyde, rinsed in PBS, equilibrated in 70% glycerol, gently squashed beneath a cover slip (which sometimes had the effect of distorting relative allantoic lengths), and viewed and photographed using a compound microscope.

Cell counts, mitotic index (MI) and morphological measurements

Cell counts and mitotic index were from sagitally oriented histological sections (4-μm thickness) and were calculated in the entire allantois as previously reported (Downs and Bertler, 2000), except that distal, mid- and proximal domains were not distinguished, and ImageJ software (National Institutes of Health, Bethesda, MD) was used to visualize the sections. The boundary between the allantois and the primitive streak was previously diagrammed (Downs and Harmann, 1997). Boundaries with the allantois and the node defined the posterior and anterior limits of the primitive streak, respectively. Within this domain, the primitive streak was taken as dense tissue where clear boundaries between epiblast and mesoderm were absent. Measurements of allantoic length for ascertaining the Vcam1 domain were carried out as previously described (Downs et al., 2004). Statistical significance of T^C/+ and T^C/T^C compared with +/+ (Fig. 3B-D, Fig. 4D,E, and Fig. 5A, part d) was assessed by two-way Student's *t*-test; equal variances were assumed, and the significance level (*P*) was taken as ≤0.05.

DiI labeling, whole embryo and explant cultures

Cell movements were traced by microinjecting a small volume (~0.5 μl) of 0.05 mg/ml CellTracker CM-DiI (1,1′ dioctadecyl-3,3,3′,3′-tetramethylindocarbocyanine perchlorate, Molecular Probes, Eugene, OR) in 0.3 M sucrose into the midline of the posterior primitive streak. Bright-field and fluorescence images were taken immediately following injection and conceptuses were placed into whole embryo culture (WEC) (Downs, 2006). After 6 hours, conceptuses were removed from the incubator, placed in HEPES-buffered dissection medium (Downs, 2006), photographed, and returned to culture for 6 hours. At 12 hours after culture, fluorescent images were taken of the posterior end of the conceptus, first with the yolk sac intact, and then after peeling it away to expose the allantois using a Spot RT-Slider camera attached to a Nikon Diaphot inverted microscope with a G2A filter cube (excitation, 535 nm; emission, 590 nm; Chroma Technology Corporation, San José, CA). Fluorescent images were pseudocolored in Metavue and superimposed with bright field using PhotoShop 7.0 software.

Not all specimens for all genotypes contained labeled allantoic cells; labeled cells were found in the posterior primitive streak alone (*n*=1, 3 and 4 for +/+, T^C/+ and T^C/T^C, respectively), or in both the posterior streak and proximal allantois (*n*=1, 7 and 4 for +/+, T^C/+ and T^C/T^C, respectively), the latter similar to previous fate mapping this region (Smith et al., 1994).

Allantoises were explanted, cultured and processed as previously described (Downs, 2006). For halved allantoises, whole allantoises were bisected transversely or longitudinally using handcrafted glass scalpels (Beddington, 1987). To ensure orientation, initial cuts were made into the allantois while it was still attached to the posterior end of the embryo, after which all bisected pieces were released and pipetted individually into the wells of a 24-well plate. Explants were stained with antibodies against Flk1 (1:100 dilution).

For yolk sac explants, the allantois was first aspirated from the exocoelomic cavity, after which glass scalpels were used to make two cuts, one below the chorion and one above the amnion (Fig. 7B, part a). Liberated yolk sacs were placed into WEC (Downs, 2006) for 24 hours. At the end of culture, yolk sac spheres were prepared for sectional immunohistochemistry, as described above.

LysoTracker Red staining

Conceptuses (EB- to 6-s) were transferred to WEC medium containing 5 μM LysoTracker Red DND-99 (Molecular Probes, Eugene, OR) and 0.01 mg/ml Hoechst (bis-benzimide, Sigma H33258) for 30 minutes. After labeling, conceptuses were rinsed three times in dissection medium, then in PBS, and fixed in 4% paraformaldehyde at 4°C for 1 hour. Following fixation, conceptuses were rinsed in PBS and equilibrated in 70% glycerol. Allantoises were isolated and gently squashed beneath a coverslip, which sometimes had the effect of distorting relative allantoic lengths. To assess cell death in the primitive streak, 6 μm transverse sections were prepared as above on samples at each of the EB, LB, EHF, LHF and 1-s stages. After dewaxing, Hoechst-stained nuclei were imaged using a DAPI/Hoechst/AMA filter cube (excitation, 360 nm; emission, 469 nm; Chroma) and LysoTracker was detected with a G2A cube. As reported in other studies (Ghatnekar et al., 2004; Zucker et al., 1999), pilot experiments in B6CBA/J F2 conceptuses confirmed the specificity of LysoTracker Red uptake. Briefly, apoptotic cells were detected in B6CBA/J F2 conceptuses primarily within the neurectoderm (LB to LHF stages), with a few positive cells in the allantoic core (data not shown). Amongst the three genotypes of the STOCK-T^C/J^{Down} strain, no differences in cell death were observed within the primitive streak (data not shown). Thus, subsequent evaluation of cell death in T^C/T^C mutants focused on the allantois.

RNA isolation and RT-PCR

Anterior tissue beneath the heart was cut by means of glass scalpels and used for genotyping, after which conceptuses were individually snap-frozen, and pooled by stage and by genotype (3-5 conceptuses/stage/genotype) during RNA isolation using the RNeasy Micro Kit (Qiagen, Valencia, CA). Total RNA (100 ng) served as template in all reverse-transcription PCR reactions (Access RT-PCR kit, Promega, Madison, WI) using gene-specific, intron-spanning primers. Primers were: *T* or T^C, 5′-TGCTGCAGTCCCATGAT-AAC-3′, 5′-CCCCTTCATACATCGGAGAA-3′; β-actin, 5′-ATGAAGAT-CCTGACCGAGCG-3′, 5′-TACTTGCGCTCAGGAGGAGC-3′. Cycling

conditions were 35 cycles of 94°C for 30 seconds, 60°C for 1 minute and 68°C for 2 minutes. Five percent of the reaction was run on a 4% GQA Sieve agarose gel.

RESULTS

A mutant T^C transcript and transient protein product are produced in T^C/T^C mutants

Results of DNA analysis and genetic studies (Herrmann and Kispert, 1994; MacMurray and Shin, 1988; Stott et al., 1993) have suggested that the T^C allele produces a mutant gene product. To clarify the status of T^C expression in homozygotes used in this study, RT-PCR was carried out on total RNA from +/+, T^C/+ and T^C/T^C conceptuses using primers that flanked the T^C deletion and thus distinguished T from T^C transcripts (see Materials and methods). A single T transcript was detected in +/+ samples, T and T^C transcripts were detected in T^C/+ samples, and a single T^C transcript was detected in T^C/T^C samples at all stages examined (LHF- to 8-s in +/+ and T^C/+; LHF- to 5-s in T^C/T^C; Fig. 1A).

Immunohistochemistry was then carried out on sectioned material. The antibody used recognizes a peptide sequence at the N terminus of T and, although not capable of distinguishing between T and T^C gene products, it can detect the unaltered N terminus of T^C. T and T^C protein was observed in all recently described sites at the EB stage (Inman and Downs, 2006) in +/+ and T^C/T^C conceptuses, respectively (Fig. 1B, parts a,c), including the primitive streak and ectoplacental endoderm (data not shown), but, in accord with our previous findings, not in the allantois at this stage. With the exception of the ectoplacental endoderm, where high levels of T^C protein persisted in the cytoplasm of this tissue (data not shown), T^C was absent in all sites in the T^C/T^C conceptus between the EHF- to 4-s stages, at which point we ended this study (e.g. Fig. 1B, parts b,d; data not shown). No differences were noted in protein localization between +/+ and T^C/+ embryos at these stages. We conclude that the T^C transcript and protein are produced in T^C/T^C conceptuses, and that the protein is initially correctly localized but, with the exception of ectoplacental endoderm, it is not maintained in the homozygous mutants.

Allantoic dysmorphogenesis is associated with reduced cell proliferation

T^C/T^C conceptuses were examined prior to embryonic death (Table 2). Although gross defects included an absence of somites (~8.25 dpc), and failure of chorio-allantoic union (~8.5 dpc), axial rotation (~9.0 dpc) and mid-/hindgut and neural tube closure (~9.5 dpc; data not shown), the earliest discernible gross defect was a short, misshapen allantois at the EHF stage (data not shown). No gross differences were noted for any feature between T^C/+ and +/+ conceptuses during this period of development.

The remainder of our study focused on T-related allantoic defects. Allantoic dysmorphogenesis was examined between the onset of appearance of the bud and 1-s (Fig. 2). Although they emerged from the appropriate site at the correct developmental time (~7.25 dpc), T^C/T^C allantoic buds were immediately less pronounced than those of +/+ littermates (data not shown). By the EHF stage, it was evident that, rather than elongating toward the chorion, T^C/T^C mutant allantoises tended to spread toward the amnion (Fig. 2A,D), making display of the entire length of mutant allantoises in any given histological section impossible (Fig. 2, compare A-C with D-F). Flattening of the allantoic projection seemed to be due to loss of the allantoic core (Fig. 2, compare A-C with D-F), which normally contained T (Fig. 1B, parts b,e-g). Thereafter, the homozygous mutant T^C/T^C allantois appeared to consist predominantly of outer mesothelial cells and some underlying core cells, few of which showed signs of endothelialization, which is typically seen in the distal allantoic region by 1-s (Downs et al., 1998) (Fig. 2, compare C with F).

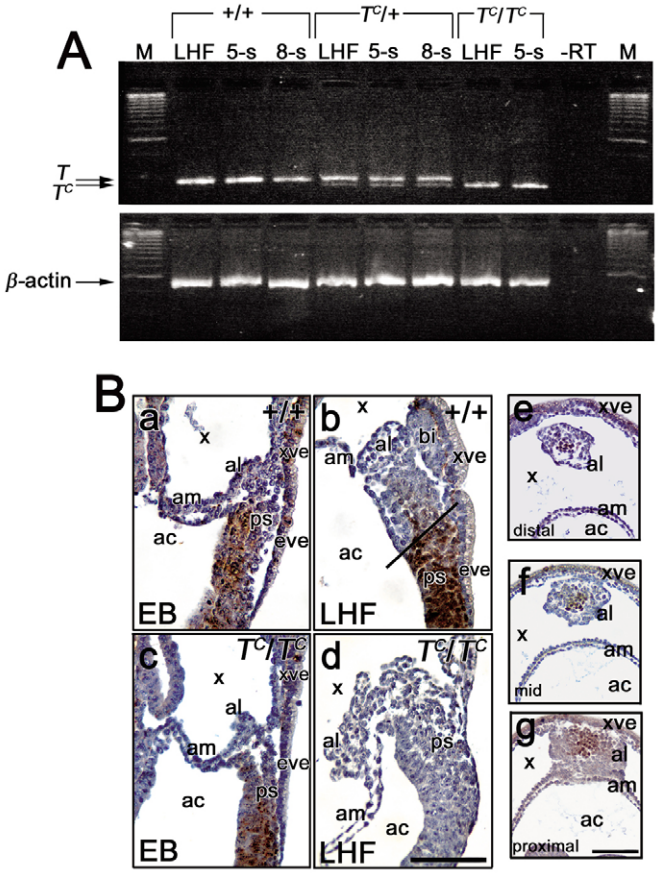

Fig. 1. T^C/T^C homozygous mutants produce a single but persistent mRNA transcript and transient protein. (**A**) RT-PCR reactions for +/+ (LHF to 8-s), T^C/+ (LHF to 8-s) and T^C/T^C (LHF, 5-s) conceptuses. A single T transcript was detected in +/+ samples, a strong T and a faint T^C band were detected at all stages in T^C/+ samples, and a single T^C transcript was detected in T^C/T^C samples. Minus reverse-transcriptase (–RT) control was negative for all reactions. M indicates marker, a 100 bp gene ruler. β-actin RT-PCR product was used as a loading control for each corresponding T RT-PCR reaction. (**B**) Immunohistochemical detection of T and T^C (brown) in +/+ (a,b) and T^C/T^C (c,d) conceptuses in sagittally oriented histological sections. T (a) and T^C (c) were localized to the primitive streak (ps) at the EB stage. At LHF, T (b) was localized to the allantoic core and primitive streak, and, with the exception of the ectoplacental endoderm (not shown), T^C (d) was not detected in the T^C/T^C conceptus. The slanted black line in b indicates the previously defined boundary between the allantois and posterior primitive streak (Downs and Harmann, 1997). (e-g) Transverse immunohistochemical sections (6 μm) through a 2-s allantois to highlight the T-defined core domain. The total length of this allantois was 258 μm after fixation. (e) The distalmost T(+) section at 102 μm (39.5% of the total fixed allantoic length). (f) A mid-region section at 48 μm. (g) The most proximal section at 6 μm. ac, amniotic cavity; al, allantois; am, amnion; bi, yolk sac blood island; eve, embryonic visceral endoderm; ps, primitive streak; x, exocoelomic cavity; xve, extraembryonic visceral endoderm. Scale bars: in d, 100 μm for a-d; in g, 100 μm for e-g.

As the primitive streak contributes cells to the allantois throughout the latter's pre-chorionic fusion stages (~7.25-8.5 dpc) (Downs and Bertler, 2000; Kinder et al., 1999; Tam and Beddington, 1987), with

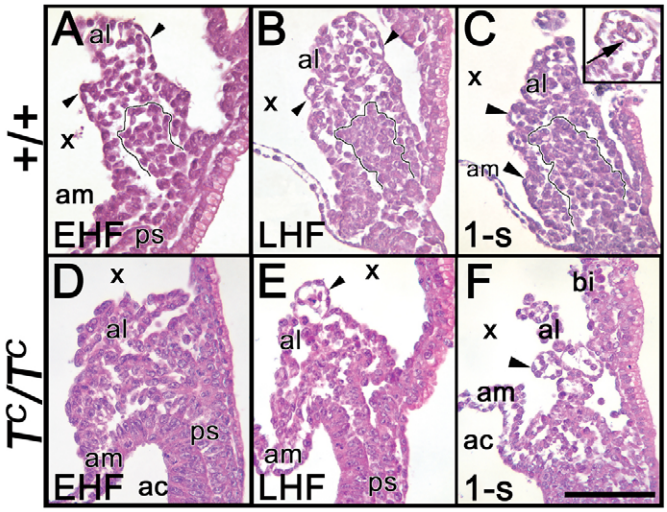

Fig. 2. Allantoic dysmorphogenesis and absence of endothelialization in T^C/T^C allantoises. (**A-F**) Hematoxylin and eosin-stained sections of allantoises (al) in +/+ (A-C) and T^C/T^C (D-F) conceptuses. Mesothelial cells (arrowheads) were observed in +/+ and T^C/T^C allantoises. The dense core of +/+ allantoises (black outline, A-C) was not clearly established or maintained in T^C/T^C. By 1-s, +/+ allantoises exhibited signs of endothelialization in distal regions (inset, C, arrow), a feature that was not readily apparent in T^C/T^C. Abbreviations as in Fig. 1. Scale bar in F: 100 μm for A-F.

the largest number added at headfold stages (Downs and Bertler, 2000; Downs et al., 2004), we investigated the possibility that T^C/T^C allantoic stunting involved a failure of cell displacement from the streak into the allantois. EHF-stage posterior streak cells of +/+, $T^C/+$ and T^C/T^C conceptuses were labeled with the fluorescent lineage tracer DiI (Fig. 3A). In all genotypes, labeled descendants were observed in the proximal allantois in some specimens after 12 hours of culture (Fig. 3A; data not shown; see Materials and methods for further explanation). Thus, T^C/T^C cells were capable of exiting the primitive streak and entering the allantois throughout the period of allantoic elongation.

Although the mitotic index (MI) of T^C/T^C allantoises was similar to +/+ at the EB stage, it was significantly decreased by the LB-EHF transition (Fig. 3B, part a) such that, by the EHF stage, a striking reduction in cell number was observed (Fig. 3C). By the LHF stage, T^C/T^C allantoises were significantly shorter than +/+ (Fig. 3D). $T^C/+$ allantoises also exhibited a reduction in length that correlated with the onset of reduced cell numbers (Fig. 3C,D). Although numbers of $T^C/+$ cells increased thereafter, wild-type levels were never achieved (Fig. 3D). In accordance with this observation, the MI of $T^C/+$ allantoises was intermediate between those of +/+ and T^C/T^C (Fig. 3B, part a). By contrast, neither cell number nor MI in the primitive streak of $T^C/+$ or T^C/T^C conceptuses differed significantly from +/+ at any stage examined (Fig. 3B, part b; data not shown).

Thus, decreased cell proliferation resulted in reduced cell numbers in T^C/T^C allantoises. However, as the MIs were calculated in sagitally sectioned material to make direct comparisons with a previous study (Downs and Bertler, 2000), we could not accurately calculate the MI in nascent streak mesoderm and, thus, could not conclude whether defective allantoic proliferation originated within nascent streak mesoderm prior to entering the allantois, or whether the proliferation defect was allantois-limited.

The allantoic core dies in the absence of T

Given that *T* was expressed within the allantoic core, we investigated whether the core domain was maintained in the mutants. The specificity of uptake of the acidotropic dye LysoTracker Red as a marker of apoptosis was verified by comparison with activated caspase-3 in pilot experiments (see Materials and methods; data not shown). Patterns of cell death in mutant allantoises were then assessed using LysoTracker Red in whole-mount preparations (Fig. 4A), and the apparent sites of expression were subsequently confirmed by sectional analysis (data not shown). At 1-s, dying cells were found within the T^C/T^C allantois, initiating in the mid-region of the allantoic core (Fig. 4A, parts a,b). By 3-s, these extended along the entire length of the core, including the distal-most part of the T^C/T^C allantois (Fig. 4A, parts f,g). By 6-s, mutant allantoises were much reduced in size compared with +/+ and only a few apoptotic cells were observed (Fig. 4A, parts h,j). At all stages, apoptosis was rare in mesothelium and immediately subjacent cell layers of the T^C/T^C allantois. In $T^C/+$ allantoises, cell death was also confined to the core at 1-s, although it was more variable and less robust than in T^C/T^C (Fig. 4A, compare parts c-e with b). By 6-s, cell death was minimal in both $T^C/+$ and T^C/T^C allantoises, and was indistinguishable from +/+ allantoises (Fig. 4A, parts h-j).

T does not affect the formation of mesothelium or chorio-adhesive cells

Collectively, our data suggest that T maintains the allantoic core. Loss of the core coincides with failure of the allantois to elongate toward the chorion. However, loss of the core did not appear to affect formation or maintenance of the outer layer of mesothelium. We had previously demonstrated that bone morphogenetic protein 4 (Bmp4), required for formation of the allantois (Winnier et al., 1995), is first expressed in the allantoic mesothelium and underlying several cell layers until about 4-s, after which expression extends to allantoic blood vessels (Downs et al., 2004; Lawson et al., 1999). As judged by sectional immunohistochemistry in the current study, Bmp4 was present in all cells remaining in T^C/T^C allantoises at intensities similar to +/+ and $T^C/+$ (Fig. 4B, parts a-d); comparison of Bmp4 expression patterns in T^C/T^C with +/+ further highlighted the loss of the allantoic core.

To provide additional support for the presence of mesothelium in the T^C/T^C mutants, we next examined Vcam1, which identifies the distal chorio-adhesive mesothelial subpopulation that mediates union with the chorion (Downs and Gardner, 1995; Gurtner et al., 1995; Kwee et al., 1995). We had previously demonstrated that the Vcam1 domain is maintained at a distance of ⩾220 μm from the primitive streak (Downs et al., 2004). In contrast to +/+ and $T^C/+$ allantoises at 5-s (Fig. 4C, part a; data not shown), Vcam1 was not detected in T^C/T^C allantoises at equivalent stages (Fig. 4C, part b), despite correct localization within the myocardium of the heart (Gurtner et al., 1995; Kwee et al., 1995) (Fig. 4C, part b, inset). These results initially suggested that *T* was in the same pathway as *Vcam1*, acting upstream of it in an allantois-specific manner. However, after measuring it, we found that the 5-s T^C/T^C allantois was not long enough to exhibit Vcam1 (Fig. 4D). By 8- to 16-s (~8.5-9.25 dpc), T^C/T^C mutant allantoises had exceeded 220 μm and contained Vcam1 (Fig. 4C, parts c,d; Fig. 4D,E), although they never elongated far enough to contact the chorion.

Thus, these results suggest that, could T^C/T^C allantoises elongate far enough, they might fuse with the chorion. However, we, and others, have recently demonstrated the presence of *T* mRNA (Rivera-Perez and Magnuson, 2005) and protein (Inman and Downs, 2006) in extraembryonic ectoderm and its derivative, chorionic

ectoderm (Inman and Downs, 2006), during the allantoic fusion period, suggesting that T may have a role in chorio-allantoic union. Thus, chorio-allantoic fusion may nonetheless be precluded in homozygous T^C/T^C mutants because of chorionic defects, a possibility that awaits further investigation.

Angioblasts are reduced in T^C/T^C mutant allantoises

Because a major function of the allantois is to establish the umbilical vasculature, we next investigated whether loss of the allantoic core prevented differentiation of allantoic mesoderm into blood vessels. In accordance with previous results (Downs et al., 1998), Flk1 was detected in scattered cells throughout the allantoic core of +/+ and T^C/+ allantoises at the EHF stage (Fig. 5A, parts a,b). Despite decreased cell numbers in T^C/+ allantoises at this stage (Fig. 3C), the percentage of Flk1-positive angioblasts did not differ significantly from +/+ (Fig. 5A, part d). By contrast, although Flk1 was correctly localized to T^C/T^C core cells (Fig. 5A, part c; data not shown), the percentage of Flk1-positive angioblasts was significantly reduced (Fig. 5A, part d).

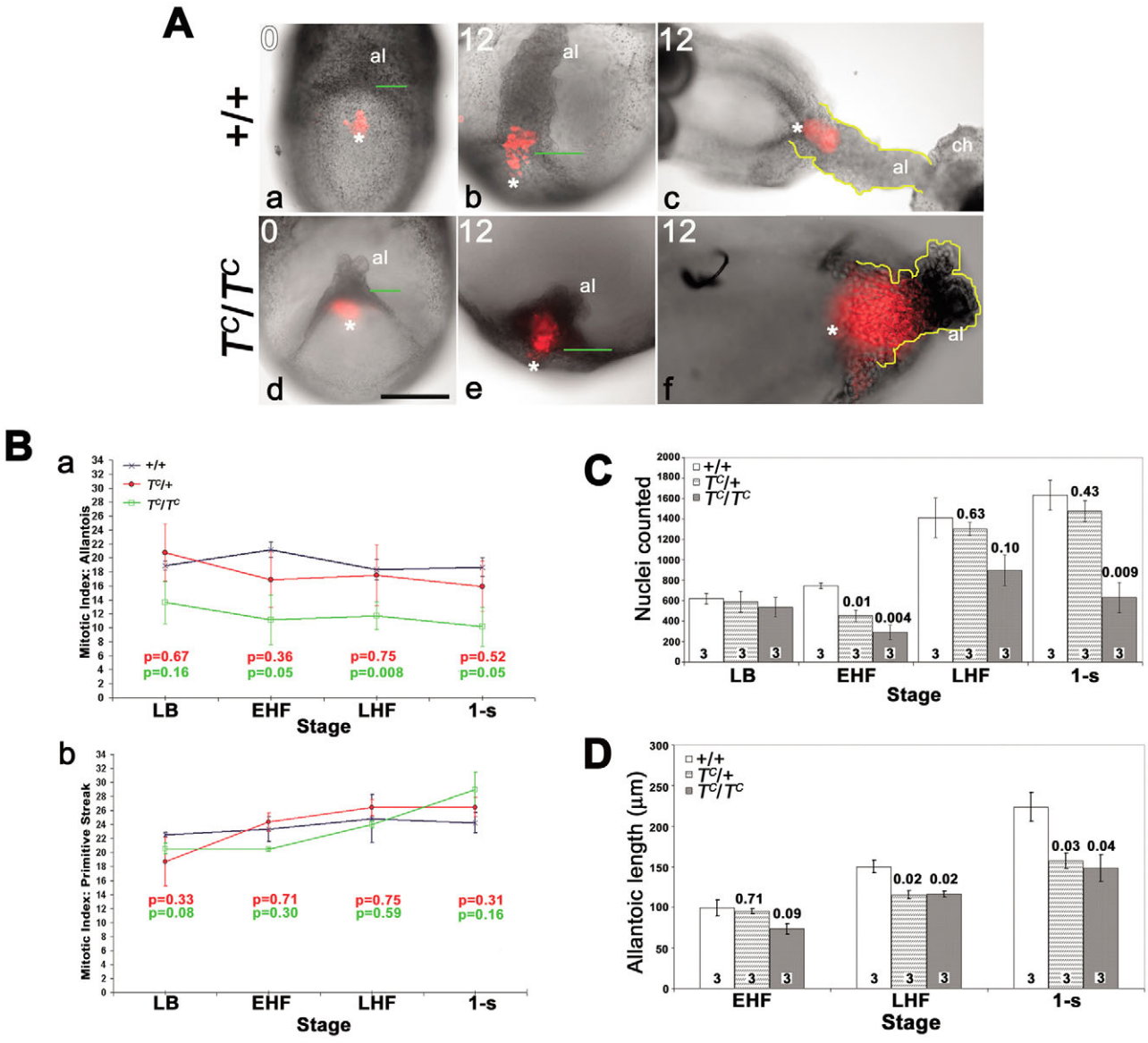

Fig. 3. Migration of mesoderm into T^C/T^C allantoises from the primitive streak is normal, but proliferation, cell number and allantoic length are reduced. (**A**) Whole-mount images of the allantois (al) and primitive streak (asterisk) at the time of (a,d) and 12 hours after (b,c,e,f) injection of DiI (red) into the primitive streak of +/+ (a-c) and T^C/T^C (d-f) EHF conceptuses. (a,b,d,e) Live images of the posterior end (up) through the yolk sac; (c,f) live images of the dorsal allantoic surfaces after the yolk sac was peeled away. The green line in a,b,d,e represents the boundary between the allantois and primitive streak; the yellow line in c,f outlines the extent of the allantois. Scale bar in d: 500 μm for a-e, 250 μm for f. al, allantois; ch, chorion. (**B**) Mitotic index (MI) calculated for the allantois (a) and primitive streak (b) for +/+, T^C/+ and T^C/T^C genotypes over the ~6-hour window during which allantoic length and cell number were reduced in T^C/T^C. Error bars represent s.e.m.; *P*-values for each mutant genotype with respect to +/+ are reported below each data point. (**C**) Bar graph of allantoic nuclei counts in +/+, T^C/+ and T^C/T^C genotypes for the interval LB to 1-s. (**D**) Bar graph of allantoic lengths (in μm) in +/+, T^C/+ and T^C/T^C genotypes for the interval EHF to 1-s. In C and D, error bars represent the s.e.m.; *P*-values for the mutant genotypes with respect to +/+ are reported above each bar.

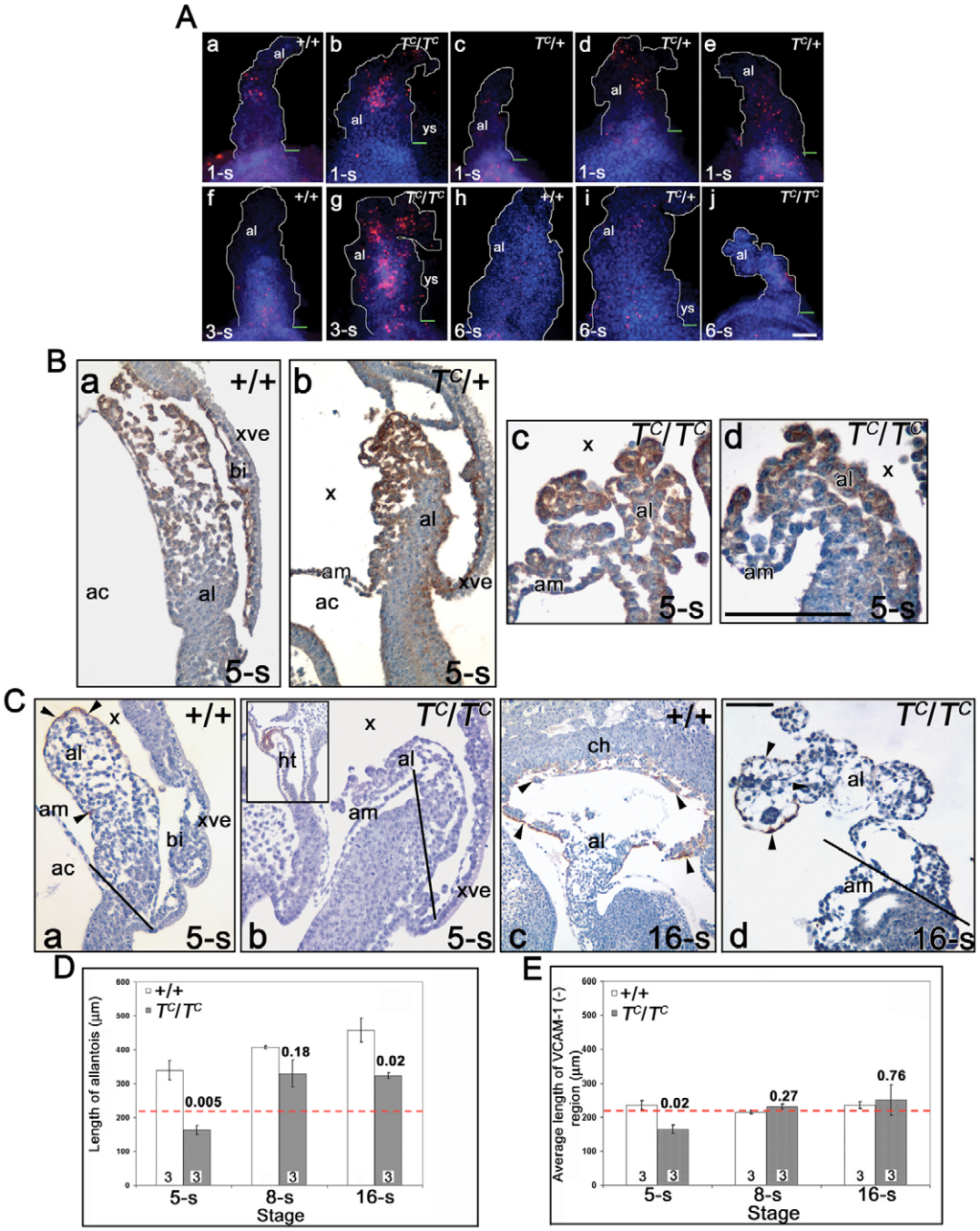

Fig. 4. Loss of T results in loss of the allantoic core but maintenance of the allantoic mesothelium and chorio-adhesive cells. (**A**) Cell death in +/+, T^C/+ and T^C/T^C whole-mount allantoises assessed by LysoTracker Red (pink signal) at 1-s (a-e), 3-s (f,g) and 6-s (h-j). Nuclei (blue) were labeled with Hoechst. White line in each panel outlines the allantois; green bar marks the base of the allantois (which in panel h lies just beneath the field of view); 'ys' indicates remnants of the yolk sac after dissection to expose the allantois. Scale bar in j: 100 μm. (**B**) Immunohistochemical analysis in sections showing that Bmp4 (brown) was excluded from the dense proximal region of +/+ (a) and T^C/+ (b) allantoises, but was detected in mesothelial and several underlying cell layers. By contrast, all of the cells in the T^C/T^C allantois in distal (c) and proximal (d) regions of a single allantois were Bmp4 positive. Scale bar in d: 100 μm for c,d; 200 μm for a,b. (**C**) Immunohistochemical detection of Vcam1 in +/+ (a,c) and T^C/T^C (b,d) allantoises. (a) Vcam1 localized to distal mesothelial and core cells (arrowheads) of +/+ allantoises at 5-s, but Vcam1 was not detected in T^C/T^C (b) allantoises, although it was detected in the developing T^C/T^C heart (ht, inset in b). (c) At 16-s (~9.5 dpc), +/+ allantoises united with the chorion (ch) and contained Vcam1 in the distal mesothelial and core cells (arrowheads). (d) T^C/T^C allantoises were not fused with the chorion, but Vcam1 was observed in the distal-most mesothelium and some core cells (arrowheads). Black lines distinguish the boundary between the posterior streak and the allantois in a,b and d. Scale bar in d: 100 μm for a,b,d; 200 μm for c and inset in b. (**D**) Bar graph of allantoic length in Vcam1-stained sections reveals that T^C/T^C allantoises attain lengths >220 μm (red horizontal line), all of which contained appropriately localized Vcam1, similar to that shown in C,d. (**E**) Bar graph of Vcam1-negative regions in the same histological sections showing maintenance of the ~220 μm Vcam1-negative region in T^C/T^C specimens. Error bars represent s.e.m. in D and E; *P*-values are reported above each bar. Abbreviations as in Fig. 1.

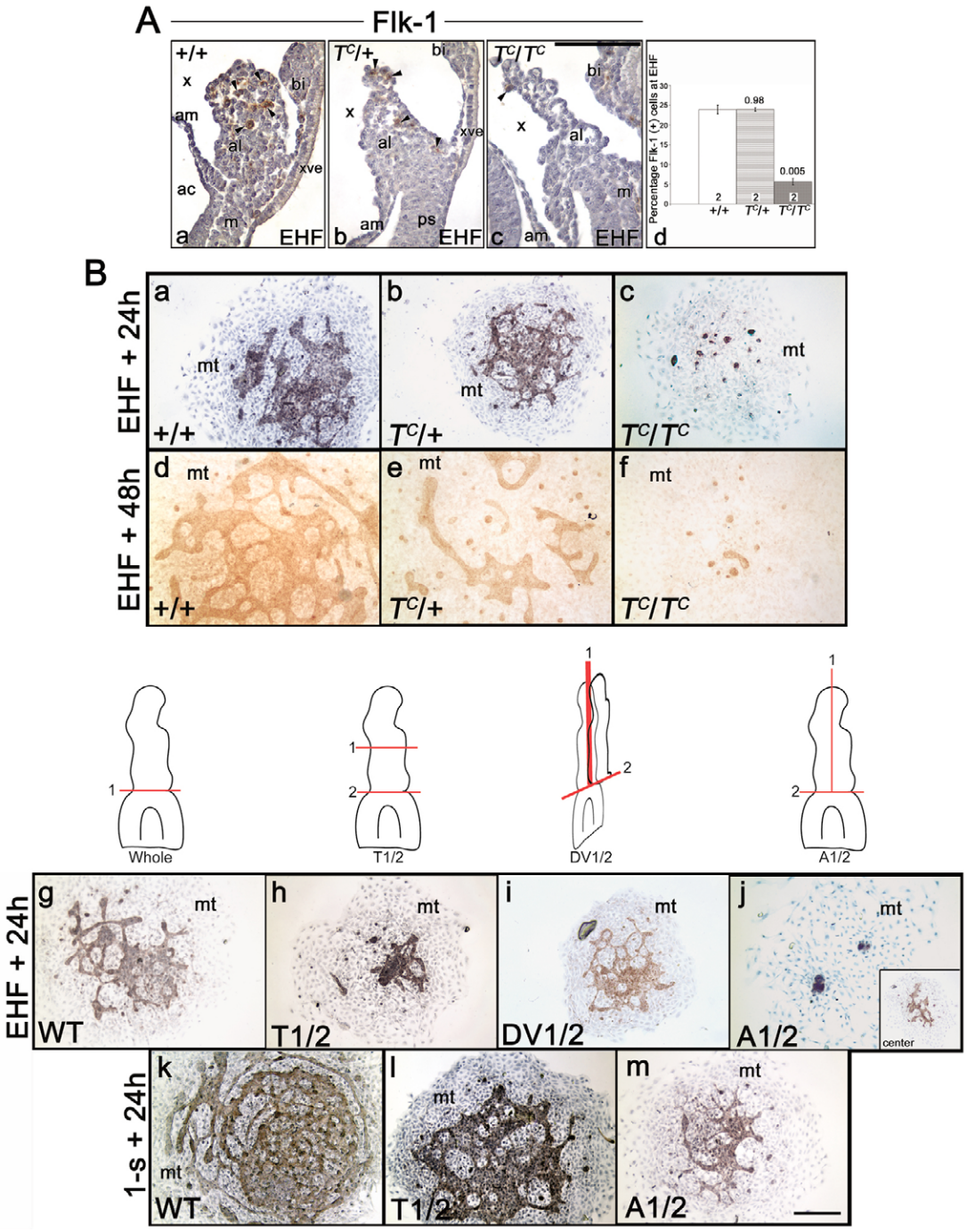

Fig. 5. The *T*-maintained allantoic core is required for expansion and coalescence of Flk1-positive angioblasts. (**A**) Immunohistochemical detection and quantification of Flk1-positive angioblasts (brown) in sections of the allantois. Flk1-positive angioblasts were prominent in the EHF distal core of +/+ (a), $T^C/+$ (b) and T^C/T^C (c) allantoises (arrowheads). (d) Bar graph showing reduced percentage of Flk1-positive cells in T^C/T^C allantoises. Error bars represent s.e.m.; *P*-values with respect to +/+ are reported above each bar. Scale bar in c: 100 μm for a-c. (**B**) Genotypes of allantoic explants are indicated at the lower left of panels a-f. Other indications at lower left (g-m) are WT (wild-type F2, see Materials and methods), transversely (T1/2) or longitudinally bisected wild-type allantoises along the presumptive dorsoventral axis (DV1/2), or axial (A1/2) plane. All explants were immunostained for Flk1 (brown) and counterstained in hematoxylin. (a-c) 24-hour allantoic explant cultures from $T^C/+$ intercross matings of EHF conceptuses; (d-f) 48-hour allantoic explants from EHF conceptuses. Schematic drawings above g-j demonstrate undivided allantoises (g) and the orientation of each plane of bisection (h-j); each corresponds to the panel directly below (g-j) and, with the exception of the DV1/2, to panels k-m. '1' and '2', and the red lines, indicate the sequence of cuts made by the glass scalpels. The tissue beneath '2' is the posterior primitive streak region. (g,k) Undivided whole allantois explant from EHF (g) or 1-s (k) wild-type conceptus. (h,l) 24-hour proximal T1/2 explants from transversely-bisected EHF (h) and 1-s (l) allantoises. (i) 24-hour EHF longitudinally bisected dorsoventral DV1/2 explants; cut '1' was made at 90° to cut '1' above j. (j,m) 24-hour explants of longitudinally bisected EHF (j) and 1-s (m) axial A1/2 allantoises. The inset in j shows vascularization in an isolated central core of an EHF-stage allantois. Scale bar in m: 500 μm (all panels in B, except for inset in j: 1,250 μm). Abbreviations as in Fig. 1. m, mesoderm; mt, mesothelial cells.

Allantoic angioblasts do not endothelialize in T^C/T^C mutants

To examine the endothelialization of T^C/T^C allantoic angioblasts, allantoises were explanted at the EHF stage and cultured in isolation for 24 hours. As judged by morphology and Flk1 immunohistochemistry, no obvious differences were detected between +/+ and T^C/+ explants (Fig. 5B, parts a,b). Explants consisted of an adherent layer of mesothelial-derived cells (Downs et al., 2004) on top of which was an expanded Flk1-positive vasculature. By contrast, the majority of cells in the T^C/T^C explant were mesothelial, the cell population that did not die in intact T^C/T^C allantoises (Fig. 5B, part c). Although some angioblasts were present, assembly into a vascular plexus was not observed.

Explants were then cultured for 48 hours, after which +/+ explants displayed expansion of the Flk1-positive plexus into an interconnected series of endothelial cell tubules (Fig. 5B, part d). Within the T^C/+ explants, elongated Flk1-positive tubules were present, but they were discontinuous and not assembled into an interconnected plexus (Fig. 5B, part e). By contrast, there was little difference in T^C/T^C explants at 48 hours compared with those at 24 hours (Fig. 5B, part f), suggesting that failure to form a vascular plexus in the mutant was not simply an issue of delayed timing. $VEGF_{165}$, added to the culture medium (Downs et al., 2001), did not rescue angioblasts or endothelialization and therefore had no discernible effect on the mutants (data not shown).

Disruption of the allantoic core phenocopies the T^C/T^C vascularization defect

As a 'community effect' is required for cell populations to achieve localized threshold levels of factors required for differentiation (Gurdon et al., 1993), we investigated whether a reduced starting population of Flk1-positive angioblasts in T^C/T^C explants was the reason for the failed vasculogenesis. To decrease overall allantoic cell number, wild-type EHF-stage allantoises were microsurgically bisected transversely (T1/2; Fig. 5B, part h) or longitudinally, either in direct register with the embryonic axis [axial halves (A1/2); Fig. 5B, part j], or at 90° with respect to this axis [presumptive dorsoventral halves (DV1/2); Fig. 5B, part i]. Each half was then plated in isolation. Previous results had demonstrated that, although the distal half of the EHF-stage allantois contained more Flk1-positive angioblasts, the base contained more cells (Downs et al., 1998). However, although careful systematic experiments of allantoises in transverse section have not been carried out to identify distinct dorsoventral or left-right allantoic coordinates, no obvious differences in Flk1 localization had previously been noted in the presumptive dorsoventral or left-right allantoic domains (Downs et al., 1998). Thus, at the outset, longitudinal explants, whatever their polarity relative to the embryonic axis, were assumed to contain roughly equivalent numbers of cells and Flk1-positive angioblasts.

All EHF-stage T1/2 and DV1/2 bisected explants formed convincing vascular plexi, although these were smaller than wild type (Fig. 5B, parts g-i). Not unexpectedly, as the mesothelium crawls off the allantois and forms a cell base onto which the vasculature adheres (Downs et al., 2004), allantoic halves contained roughly half the amount of mesothelium as whole allantoises. In striking contrast, all A1/2 explants exhibited a failure of vasculogenesis similar to that seen in T^C/T^C explants (Fig. 5B, part j). Preservation of the central axial allantoic core resulted in normal vascularization (Fig. 5B, part j, inset). Thus, we conclude that, rather than a reduction in cell number, perturbation of the T core domain appears to affect allantoic endothelialization, but only along the axis of bilateral symmetry that is in register with the AP axis of the embryo.

To determine whether perturbation to the axial allantoic core was specific to the headfold stage, we then longitudinally bisected allantoises at slightly later stages when these bore morphological evidence of endothelialization (Downs et al., 1998; Downs et al., 2004). Although older A1/2 explants were not as robust as undivided EHF-stage and T1/2 explants, they did form an endothelialized vascular plexus similar to those found in +/+ and T^C/+ (Fig. 5B, parts k-m). Thus, once angioblast clustering and endothelialization had begun, disruption of the axial core did not have a striking effect on plexus formation. We conclude that the axial core does not play a role in the formation of mesothelium but profoundly affects angioblast survival and endothelialization.

Absence of Pecam1 and vascular patterning in T^C/T^C mutant allantoises

In contrast to Flk1, which is scattered throughout the allantoic core during pre-fusion stages (see Downs et al., 2004), Pecam1 has been observed anecdotally within a central midline vessel of the allantois as early as headfold stages (Ilic et al., 2003; Naiche and Papaioannou, 2003). Pecam1 is a member of the immunoglobulin (Ig) superfamily, containing a cytoplasmic immunoreceptor tyrosine-based inhibitory motif (ITIM), and playing roles in endothelial cell survival and migration (Newman, 1999; Newman and Newman, 2003). Pecam1 is dispersed across the cell surface in migrating endothelial cells, but localizes to endothelial cell intercellular junctions in non-migrating cells (Gratzinger et al., 2003; Newman et al., 1992; Wong et al., 2000). The spatial relationship between Pecam1 and Flk1 is not known, but, given that the allantoic core died in T^C/T^C mutants, and that numbers of Flk1 angioblasts were severely diminished, we examined Pecam1 first in wild-type allantoises whose Flk1 angioblasts were marked with a reporter *lacZ* construct ($Flk1^{lacZ}$; see Materials and methods), and then in littermates of T^C/+ intercrosses.

Pecam1 was initially observed in a clustered group of allantoic cells at the LB stage, whereas Flk1 angioblasts, as described previously, were scattered throughout the core (Fig. 6A, part a, inset). From the LB cluster, the Pecam1 domain extended distally (Fig. 6A, parts a,b), forming a central vessel that showed signs of increased branching with increasing age (Fig. 6A, part c). At 2-s, the central track of proximal Pecam1 seemed to split and triangulate around the proximal allantoic core (Fig. 6A, part b), but, by 6-s, it formed a robust central vessel that had amalgamated with the embryonic dorsal aorta (Fig. 6A, part c). Between 2- and 6-s, Pecam1 was most clearly observed on the cell surface, outlining individual cells (e.g. Fig. 6A, part c). Intriguingly, Flk1-positive angioblasts did not coalesce into a central vessel and amalgamate with the embryonic vasculature until 6-s (Fig. 6A, part d). Thus, in contrast with Flk1, Pecam1 defines a spatially patterned vascular domain in the allantois between ~7.25 and 8.5 dpc.

In +/+ littermates of T^C/T^C mutants, Pecam1 was detected along the central allantoic vessel, where it was also present on the cell surface, as well as on the surface of the developing dorsal aortae of the embryo (Fig. 6B, part a and inset). In T^C/+ allantoises, the Pecam1-positive vessel was present but of variable length, and Pecam1 staining was absent in the dorsal aortae (Fig. 6B, parts b,c). Given that T^C/+ pups are viable, these observations may reflect a delay in vasculogenesis. Neither the Pecam1-positive allantoic midline nor dorsal aortae were observed in T^C/T^C conceptuses at the stages examined (2- and 5-s), although an occasional Pecam1-

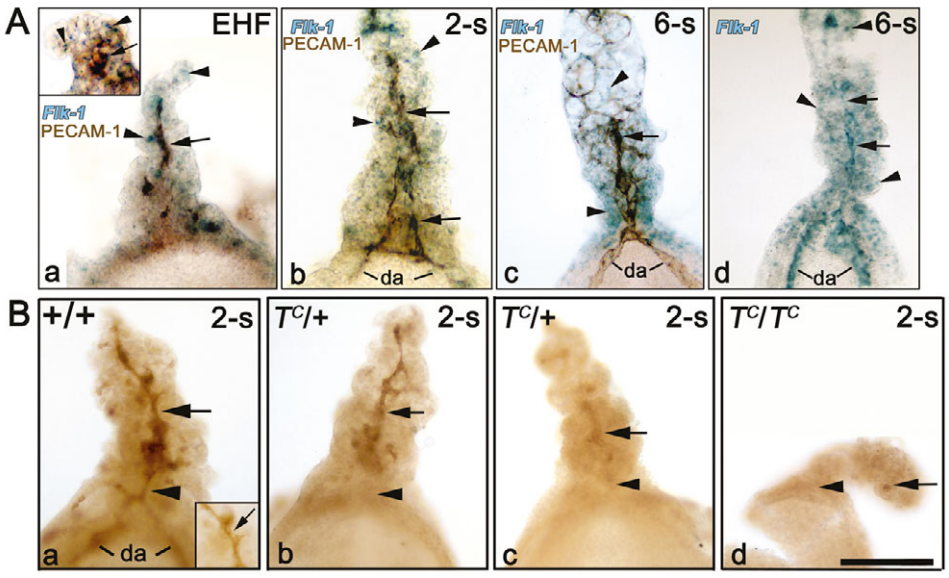

Fig. 6. Pecam1 identifies a nascent vascular scaffolding that is missing in T^C/T^C allantoises. (**A**) Whole-mount Pecam1 (brown) and Flk1 (X-gal, blue) in Flk^{lacZ} conceptuses (see Materials and methods). (a) Pecam1 (arrows) was detected in a small cluster as early as the LB stage (inset), whereas *lacZ*-positive cells were dispersed in the allantois (arrowheads in this and all panels in A). By the EHF stage, Pecam1 defined a central vessel that extended distally and proximally (a-c), and ultimately converged upon the developing embryonic dorsal aortae (da; c). Flk1-positive cells were not localized to a patterned central vessel until 6-s (d). (**B**) Pecam1 detection in +/+ (a) (inset shows localization on the cell surface), $T^C/+$ (b,c), and T^C/T^C (d) 2-s conceptuses. Formation of the Pecam1-positive central vessel (arrows in a-c) was variable in $T^C/+$ allantoises. A single Pecam1-positive cell was detected in the T^C/T^C allantois (arrow in d). Pecam1 was not detected in the posterior embryonic region of $T^C/+$ or T^C/T^C conceptuses (arrowheads mark the site where continuity with the embryonic dorsal aortae was expected). Scale bar in B, part d: 100 μm for A, parts a,b, B parts a-d; 250 μm for A, parts c,d; 25 μm for inset in A, part a; 50 μm for inset in B, part a.

positive cell was found in the distal T^C/T^C allantois (Fig. 6B, part d). Thus, we conclude that, although T is not required for the differentiation of Flk1 or Pecam1 angioblasts, its absence results in loss of vascular patterning in the allantois.

T plays a global role in vascularization throughout the conceptus

The allantois/umbilical, yolk sac and cardiovascular systems represent the three major vascular systems in the conceptus. Our breeding data revealed that T^C/T^C embryos died between ~9.5 and 10.5 dpc (Table 2), slightly earlier than presumptive embryonic dependence on the chorio-allantoic placenta, and coinciding more precisely with activity of the chorio-vitelline placenta (Copp, 1995) and the presence of a robust circulation (Downs et al., 1998). As T protein was recently described within the developing heart and within the extraembryonic visceral endoderm overlying nascent blood islands of the yolk sac (Inman and Downs, 2006), we examined these major vascular organs for evidence of aberrancies in T^C/T^C mutant conceptuses.

Until 2- to 3-s, the developing T^C/T^C heart field was grossly indistinguishable from +/+ (data not shown). As early as 4-s, when T was first observed in the heart (Inman and Downs, 2006), histological sections of T^C/T^C hearts revealed a reduced cardiogenic mass (data not shown). By 6-s, when levels of T were maximal in myo- and endocardium (Inman and Downs, 2006), the heart appeared dysmorphic, exhibiting a decreased pericardial cavity, and reduced myo- and endocardium (Fig. 7A, parts a,b). In contrast to +/+, only low levels of Flk1 were detected in the mutant myocardium (Fig. 7A, parts a,b). By 16-s (~9.5 dpc), large numbers of pyknotic cells were observed in T^C/T^C hearts (data not shown). Similar to previous results in *T/T* mice (King et al., 1998), defects in T^C/T^C hearts were observed during the time of heart looping and involved structural abnormalities of developing heart layers.

In addition, aberrant T^C/T^C yolk sac blood island morphology was observed in some histological sections as early as the EHF stage when T was recently reported in extraembryonic visceral endoderm overlying blood island mesoderm (Inman and Downs, 2006); however, abnormalities were most pronounced by 1-s (e.g. Fig. 2F, Fig. 5A, part c). T^C/T^C conceptuses had a thickened region in the approximate location of developing blood islands, where cells were found between the extraembryonic mesoderm and visceral endoderm layers but were not packaged inside a continuous Flk1-positive endothelium.

To examine development of mutant yolk sacs in isolation, yolk sacs of +/+, $T^C/+$ and T^C/T^C conceptuses were separated from the rest of the conceptus (Fig. 7B, part a) and cultured for 24 hours. +/+ yolk sacs exhibited continuity of the visceral endoderm, and Flk1-positive vascular channels contained an abundance of hematopoietic cells (Fig. 7B, parts b,c). By contrast, the visceral endoderm of T^C/T^C mutant yolk sacs was discontinuous, and appeared to contain an abnormally high lipophilic content within cytoplasmic vacuoles (Fig. 7B, parts d,e). Presumptive hematopoietic precursors remained in a compact cluster within discontinuous Flk1 vessels and exhibited evidence of pyknosis (Fig. 7B, parts d,e). $T^C/+$ yolk sacs exhibited a phenotype intermediate between +/+ and T^C/T^C; for example, some blood islands and associated extraembryonic visceral endoderm appeared relatively normal (e.g. Fig. 7B, part f), whereas others were dysmorphic (Fig. 7B, part g).

DISCUSSION

The starting point for the current study was the observation made over sixty years ago that homozygous brachyury (*T/T*) mutant embryos exhibited a short and misshapen allantois that did not fuse with the chorion (Gluecksohn-Schoenheimer, 1944). In that landmark study, presumptive +/+, *T*/+ and *T/T* conceptuses were explanted and cultured within the chick extraembryonic coelom to elucidate the role of the allantois in embryonic development. It was concluded, however, that the variability in the resultant *T* allantoic phenotypes and the inability to correlate genotype with each class of allantoic defect precluded an elucidation of the role of T in the allantois, and the role of the allantois in the embryo.

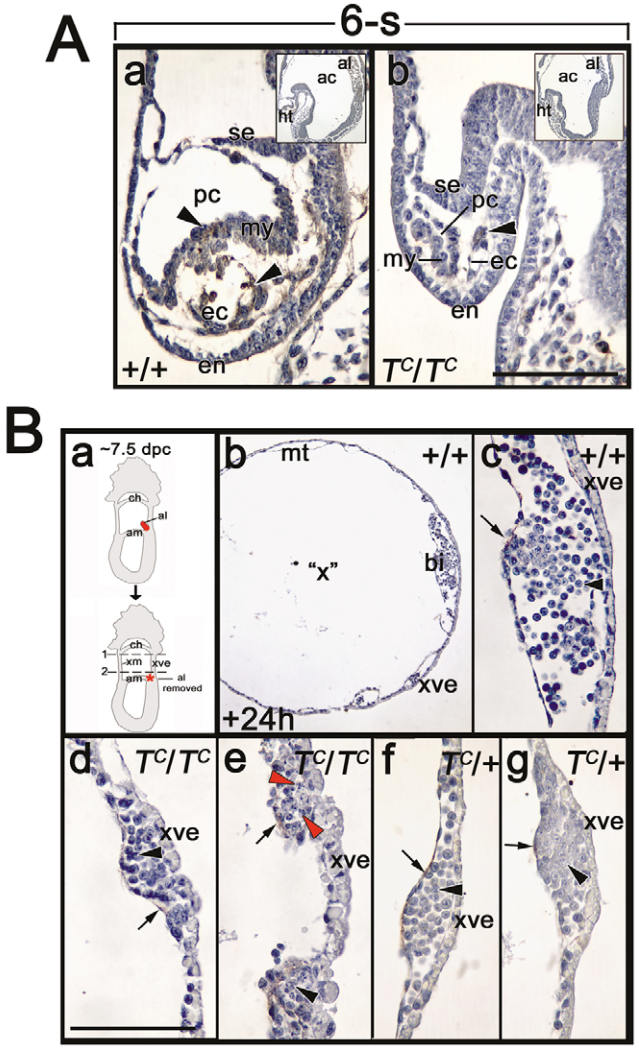

Fig. 7. T^C/T^C conceptuses exhibit defects in heart and yolk sac. (**A**) Equivalent sections (insets in a and b) of +/+ (a) and T^C/T^C (b) 6-s hearts show a reduction in the pericardial cavity (pc) and both myocardial (my) and endocardial (ec) layers in T^C/T^C. A few Flk1-positive cells (arrowheads) were observed in the T^C/T^C mutant endocardium. Scale bar in b: 100 μm for a,b. (**B**) Yolk sacs were isolated from EHF-stage conceptuses (a) and cultured for 24 hours to produce yolk sac spheres. 1 and 2 indicate the level of cuts made in the conceptus to isolate the yolk sac (see Materials and methods). (b) Histological section through a +/+ yolk sac sphere. (c-g) Higher magnification of yolk sac vasculature in +/+ (c), T^C/T^C (d,e) and T^C/+ (f,g) spheres. Flk1-positive endothelium (arrows) was discontinuous and the endoderm layer was not uniformly thick in T^C/T^C yolk sacs (compare d and e with wild type in c). Presumptive hematopoietic precursor cells (black arrowheads) were present between T^C/T^C yolk sac layers, but remained in a tight cluster and contained pyknotic cells (red arrowheads). (f,g) Two different regions of the same T^C/+ sphere reveal an intermediate phenotype (see text). Abbreviations as in Fig. 1. ht, heart; en, endoderm of foregut; se, surface ectoderm; mt, mesothelium; 'x', former exocoelomic cavity of the intact conceptus. Scale bar in d: 100 μm for c-g; 400 μm for b.

Thanks to the 'tour-de-force' molecular cloning of *T* (Herrmann et al., 1990), we were able to readily genotype conceptuses bearing $T^{Curtailed}$, a *T*-limited allele (Searle, 1966; Stott et al., 1993), and to combine this information with recent technical and intellectual advances in allantoic development. These included knowledge of the origin of allantoic mesoderm (Lawson et al., 1991), a morphological staging system (Downs and Davies, 1993), a reliable and practical method of whole embryo culture (Lawson et al., 1991), and an explant system (Downs et al., 1998; Downs et al., 2001). Moreover, we made use of an emerging developmental context for the allantois (see Downs et al., 2004).

We report that T maintains a novel allantoic core domain between the LB and 4-s stages, a period that coincides with our recent finding of robust expression of *T* in this location (Inman and Downs, 2006). We show here that, in the absence of T, the core died, resulting in a failure of the allantois to elongate toward the chorion and appropriately vascularize.

Whilst the major focus of our study was on the role of T in the allantois, our results link T function to widespread vascularization in the mouse conceptus. Although not yet extensively studied, loss of T affected development of the heart, the first signs of cardiac dysmorphology beginning at 4-s when T was first detectable in the cardiogenic mass (Inman and Downs, 2006). This finding suggests that T is required autonomously within the heart. *T* also appeared to be required for correct yolk sac vascularization, as T was identified within yolk sac endoderm (Inman and Downs, 2006). Yolk sac endoderm is required for the formation of yolk sac blood vessels in the chick (Miura and Wilt, 1970; Wilt, 1965) and yolk sac blood islands in the mouse (Belaoussoff et al., 1998). Thus, on the basis of these findings, we conclude that *T* plays a global role in vascularization of the mouse conceptus.

The T^C allele produces a mutant gene product

Previous studies indicated that the T^C deletion produces a mutant protein (Herrmann and Kispert, 1994; MacMurray and Shin, 1988) that may interfere with *T* in T^C/+ conceptuses. Dominant-negative (antimorphic) action of the T^C allele was revealed in experiments where introduction of a full-length *T* transgene failed to completely restore tail length in T^C/+ animals (Stott et al., 1993). The work presented here revealed that T^C/+ heterozygotes exhibited allantoic phenotypes intermediate between those of +/+ and T^C/T^C for all parameters examined, including allantoic elongation, cell number, mitotic index, cell death and vasculogenesis, the latter affecting the yolk sac as well. Despite being shorter than wild type, all T^C/+ allantoises ultimately grew far enough to fuse with the chorion. Thus, these results support an antimorphic nature of the T^C allele with respect to the wild-type protein product.

To provide insight into the molecular nature of T, we demonstrated that T^C expresses a single mRNA transcript that is maintained in the heterozygous and homozygous genotypes throughout the period examined here. By contrast, the T^C protein, although initially localized properly to the T expression domain, was only transiently expressed in the T^C/T^C conceptus, except within ectoplacental (distal extraembryonic) endoderm, which will line the sinuses of Duval (Duval, 1891), thought to be involved in calcium transport (Bruns et al., 1985). It was previously shown that, in *T/T* ES cells, the *T* promoter can be activated in the absence of functional T protein (Schmidt et al., 1997). Our results reveal that the unaltered promoter region of T^C is activated in vivo in a completely mutant environment. This finding is similar to reports of another *T* allele, T^{Wis} (Herrmann, 1991; Kispert and Herrmann, 1994), and supports some degree of autoregulation of *T*. A series of studies in *Xenopus* (Casey et al., 1998; Isaacs et al., 1994; Schulte-Merker and Smith, 1995) and mouse (Clements et al., 1996; Galceran et al., 2001; Yamaguchi et al., 1999) indicated an indirect autoregulatory feedback loop involving *T* and members of the fibroblast growth factor (Fgf) family (*Xenopus*) and the Wnt family (mouse). Together,

these studies proposed that Fgf and Wnt family members are targets of *T*. Furthermore, although neither Fgfs nor Wnts are required for the initiation of *T* expression, signaling from these *T* targets is required to sustain further production of T. Why the mutant T^C protein persists only in ectoplacental endoderm is not clear; although very little is known about this tissue, one possibility is that it lacks the machinery to degrade defective proteins.

T maintains a novel allantoic core domain required for allantoic elongation

As discussed in previous sections, recent results from our laboratory demonstrated that T is localized to a novel allantoic core domain between LB and 6-s (~7.25-8.25 dpc), which, as observed in sagittal section, was continuous with the embryonic primitive streak (Inman and Downs, 2006). Here, we have confirmed by transverse immunohistochemical sections that T lies within the allantoic core (Fig. 1B, parts e-g). In the absence of *T*, only the outer few allantoic cell layers were maintained. In addition, overall allantoic cell proliferation was diminished and cells in the allantoic core died. Together, these had the effect of abrogating allantoic elongation. By contrast, the primitive streak, which also expresses T, appeared normal for both cell proliferation and survival during the stages examined. That Vcam1 was correctly expressed and positioned within the distal allantoic region further supported normal streak activity, as we have previously demonstrated that positioning of allantoic Vcam1 is dependent upon signaling from the streak (Downs et al., 2004). Finally, these results provide a plausible explanation for why *T*/*T* mutant cells were not found within some defective allantoises of otherwise chimeric *T*/*T* conceptuses (Wilson et al., 1993): instead of failure to be displaced from the streak into the allantois, which we showed was not the case (Fig. 3A), *T*/*T* cells likely contributed to the allantois. In those chimeras where mutant cells had contributed to the core, the latter might have died during a developmental window that was overlooked in those previous studies.

T is not required for differentiation of mesoderm into angioblasts, but is required for vascular patterning

In the absence of *T*, angioblasts formed, but their population did not expand, either because of diminished proliferation and/or because of failure to survive. Moreover, although the odd Pecam1-positive cell was found in homozygous T^C/T^C mutant allantoises, vascular patterning, as revealed by an increasingly branched Pecam1-positive allantoic midline vessel in normal allantoises, was abolished.

Although the precise relationship between Flk1 and Pecam1 within the allantois is not yet known, our results suggest that Pecam1-positive cells provide a vascular scaffolding upon which the dispersed Flk1-positive cells can assemble. Flk1-positive cells did not form a central vessel until 6-s (Fig. 5A, part d). By contrast, Pecam1 cells immediately assembled into a central vessel that began to extend toward the embryonic region at 2-s, although its embryonic connection was not certain until 6-s (Fig. 5A-C). Amalgamation of the vascular systems of the conceptus by 6-s is consistent with previous results that demonstrated that infiltration of yolk sac primitive erythroid cells into the allantois takes place at about 5-s (Downs et al., 1998).

Localization of Pecam1 to the surface of angioblasts has been implicated in angioblast migration and assembly into cords (Bohnsack and Hirschi, 2003). This process may involve heterophilic interactions between Pecam1 and integrins (Wong et al., 2000). In addition, mutants bearing a disruption in focal adhesion kinase (FAK; Ptk2 – Mouse Genome Informatics) exhibit differentiation of angioblasts but lack an endothelialized and patterned allantoic vasculature (Ilic et al., 2003). Thus, further investigation into the molecular hierarchies involved in vascular patterning may identify integrins and FAK as downstream members of a T-activated pathway for vascular patterning.

Finally, $Vegf_{165}$, the predominant isoform of Vegfa, which has an affinity for heparin (Ferrara and Davis-Smyth, 1997), was not able to rescue T^C/T^C mutant Flk1 cells, as it did wild-type allantoic angioblasts cultured in low serum (Downs et al., 2001). Although further study is required, heparin or heparan sulfate proteoglygans may be absent from or defective in mutant allantoises, which accords with observations that *T*/*T* mutants are defective in the extracellular matrix (Jacobs-Cohen et al., 1983).

The source of the allantoic vascular patterning signal may reside within the allantoic core. Physically disrupting the core within its plane of continuity with the embryonic midline phenocopied the T endothelialization defect: angioblasts formed, but they did not endothelialize. Longitudinal bisections 90° to this axis or perpendicular to it had no affect on vascularization. Thus, these observations suggest that the allantoic core possesses polarity that is aligned with respect to the embryonic AP axis.

We thank Dr David Stott for assistance with genotyping, Dr Tom Sato for providing us with the *Flk1lacZ* male mouse, M. Cabell Jonas for help with Flk1/β-gal staining, and Professor Sir Richard Gardner for valuable comments on the manuscript. This study was carried out in partial fulfillment of the PhD degree (K.E.I.) and was supported by RO1 HD042706 from the National Institutes of Child Health and Development (K.M.D.).

References

Beddington, R. S. P. (1987). Isolation, culture and manipulation of post-implantation mouse embryos. In *Mammalian Development: A Practical Approach* (ed. M. Monk), pp. 43-70. Oxford: IRL Press.
Belaoussoff, M., Farrington, S. M. and Baron, M. H. (1998). Hematopoietic induction and respecification of A-P identity by visceral endoderm signaling in the mouse embryo. *Development* **125**, 5009-5018.
Bohnsack, B. L. and Hirschi, K. K. (2003). The FAKs about blood vessel assembly. *Circ. Res.* **92**, 255-257.
Brown, J. J. and Papaioannou, V. E. (1993). Ontogeny of hyaluronan secretion during early mouse development. *Development* **117**, 483-492.
Bruns, M. E., Kleeman, E., Mils, S. E., Bruns, D. E. and Herr, J. C. (1985). Immunochemical localization of vitamin D-dependent calcium-binding protein in mouse placenta and yolk sac. *Anat. Rec.* **213**, 514-517, 532-535.
Casey, E. S., O'Reilly, M. A., Conlon, F. L. and Smith, J. C. (1998). The T-box transcription factor Brachyury regulates expression of eFGF through binding to a non-palindromic response element. *Development* **125**, 3887-3894.
Chesley, P. (1935). Development of the short-tailed mutant in the house mouse. *J. Exp. Zool.* **70**, 429-459.
Clements, D., Taylor, H. C., Herrmann, B. G. and Stott, D. (1996). Distinct regulatory control of the Brachyury gene in axial and non-axial mesoderm suggests separation of mesoderm lineages early in mouse gastrulation. *Mech. Dev.* **56**, 139-149.
Copp, A. J. (1995). Death before birth: clues from gene knockouts and mutations. *Trends Genet.* **11**, 87-93.
Dobrovolskaia-Zavadskaia, N. (1927). Sur la mortification spontanée chez la souris nouveau-née et sur l'existence d'un caractère (facteur) hereditaire, non-viable. *Crit. Rev. Soc. Biol.* **97**, 114-119.
Downs, K. M. (2002). Early placental ontogeny in the mouse. *Placenta* **23**, 116-131.
Downs, K. M. (2006). In vitro culture model for studying vascularization in allantoic explants and allantoic fusion with the chorion. *Methods Mol. Med.* **121**, 241-272.
Downs, K. M. and Davies, T. (1993). Staging of gastrulating mouse embryos by morphological landmarks in the dissecting microscope. *Development* **118**, 1255-1266.
Downs, K. M. and Gardner, R. L. (1995). An investigation into early placental ontogeny: allantoic attachment to the chorion is selective and developmentally regulated. *Development* **121**, 407-416.
Downs, K. M. and Harmann, C. (1997). Developmental potency of the murine allantois. *Development* **124**, 2769-2780.
Downs, K. M. and Bertler, C. (2000). Growth in the pre-fusion murine allantois. *Anat. Embryol.* **202**, 323-331.
Downs, K. M., Gifford, S., Blahnik, M. and Gardner, R. L. (1998). The murine

allantois undergoes vasculogenesis that is not accompanied by erythropoiesis. *Development* **125**, 4507-4521.
Downs, K. M., Temkin, R., Gifford, S. and McHugh, J. (2001). Study of the murine allantois by allantoic explants. *Dev. Biol.* **233**, 347-364.
Downs, K. M., Hellman, E. R., McHugh, J., Barrickman, K. and Inman, K. E. (2004). Investigation into a role for the primitive streak in development of the murine allantois. *Development* **131**, 37-55.
Duval, M. (1891). Le placenta des rongeurs. Trosième partie. Le placenta de la souris et du rat. *J. Anat. Physiol. Norm. Pathol. Homme Anim.* **27**, 24-73, 344-395, 515-612.
Ferrara, N. and Davis-Smyth, T. (1997). The biology of vascular endothelial growth factor. *Endocr. Rev.* **18**, 4-25.
Galceran, J., Hsu, S. C. and Grosschedl, R. (2001). Rescue of a Wnt mutation by an activated form of LEF-1: regulation of maintenance but not initiation of Brachyury expression. *Proc. Natl. Acad. Sci. USA* **98**, 8668-8673.
Ghatnekar, G. S., Barnes, J. A., Dow, J. L. and Smoak, I. W. (2004). Hypoglycemia induced changes in cell death and cell proliferation in the organogenesis stage embryonic mouse heart. *Birth Defects Res. Part A Clin. Mol. Teratol.* **70**, 121-131.
Gluecksohn-Schoenheimer, S. (1944). The development of normal and homozygous brachy (T/T) mouse embryos in the extraembryonic coelom of the chick. *Proc. Natl. Acad. Sci. USA* **30**, 134-140.
Gratzinger, D., Barreuther, M. and Madri, J. A. (2003). Platelet-endothelial cell adhesion molecule-1 modulates endothelial migration through its immunoreceptor tyrosine-based inhibitory motif. *Biochem. Biophys. Res. Commun.* **301**, 243-249.
Gurdon, J. C., Kato, K. and Lemaire, P. (1993). The community effect, dorsalization and mesoderm induction. *Curr. Opin. Genet. Dev.* **3**, 662-667.
Gurtner, G. C., Davis, V., Li, H., McCoy, M. J., Sharpe, A. and Cybulsky, M. I. (1995). Targeted disruption of the murine VCAM1 gene: essential role of VCAM-1 in chorioallantoic fusion and placentation. *Genes Dev.* **9**, 1-14.
Herrmann, B. G. (1991). Expression pattern of the Brachyury gene in whole-mount TWis/TWis mutant embryos. *Development* **113**, 913-917.
Herrmann, B. G. and Kispert, A. (1994). The T genes in embryogenesis. *Trends Genet.* **10**, 280-286.
Herrmann, B. G., Labeit, S., Poustka, A., King, T. R. and Lehrach, H. (1990). Cloning of the T gene required in mesoderm formation in the mouse. *Nature* **343**, 617-622.
Ilic, D., Kovacic, B., McDonagh, S., Jin, F., Baumbusch, C., Gardner, D. G. and Damsky, C. H. (2003). Focal adhesion kinase is required for blood vessel morphogenesis. *Circ. Res.* **92**, 300-307.
Inman, K. E. and Downs, K. M. (2006). Localization of Brachyury (T) in embryonic and extraembryonic tissues during mouse gastrulation. *Gene Expr. Patterns* (in press).
Isaacs, H. V., Pownall, M. E. and Slack, J. M. (1994). eFGF regulates Xbra expression during Xenopus gastrulation. *EMBO J.* **13**, 4469-4481.
Jacobs-Cohen, R. J., Spiegelman, M. and Bennett, D. (1983). Abnormalities of cells and extracellular matrix of T/T embryos. *Differentiation* **25**, 48-55.
Kinder, S. J., Tsang, T. E., Quinlan, G. A., Hadjantonakis, A.-K., Nagy, A. and Tam, P. P. L. (1999). The orderly allocation of mesodermal cells to the extraembryonic structures and the anteroposterior axis during gastrulation of the mouse embryo. *Development* **126**, 4691-4701.
King, T., Beddington, R. S. and Brown, N. A. (1998). The role of the brachyury gene in heart development and left-right specification in the mouse. *Mech. Dev.* **79**, 29-37.
Kispert, A. and Herrmann, B. G. (1994). Immunohistochemical analysis of the Brachyury protein in wild-type and mutant mouse embryos. *Dev. Biol.* **161**, 179-193.
Kwee, L., Baldwin, H. S., Shen, H. M., Steward, C. L., Buck, C., Buck, C. A. and Labow, M. A. (1995). Defective development of the embryonic and extraembryonic circulatory systems in vascular cell adhesion molecule (VCAM-1) deficient mice. *Development* **121**, 489-503.
Lawson, K. A., Meneses, J. and Pedersen, R. A. (1991). Clonal analysis of epiblast fate during germ layer formation in the mouse embryo. *Development* **113**, 891-911.
Lawson, K. A., Dunn, N. R., Roelen, B. A., Zeinstra, L. M., Davis, A. M., Wright, C. V., Korving, J. P. and Hogan, B. L. (1999). Bmp4 is required for the generation of primordial germ cells in the mouse embryo. *Genes Dev.* **13**, 424-436.
MacMurray, A. and Shin, H. S. (1988). The antimorphic nature of the Tc allele at the mouse T locus. *Genetics* **120**, 545-550.
Millauer, B., Wizigmann-Voos, S., Schnurch, H., Martinex, R., Moller, N. P., Risau, W. and Ullrich, A. (1993). High affinity VEGF binding and developmental expression suggest Flk-1 as a major regulator of vasculogenesis and angiogenesis. *Cell* **72**, 835-846.
Miura, Y. and Wilt, F. H. (1970). The formations of blood islands in dissociated-reaggregated chick embryo yolk sac cells. *Exp. Cell Res.* **59**, 217-226.
Naiche, L. A. and Papaioannou, V. E. (2003). Loss of Tbx4 blocks hindlimb development and affects vascularization and fusion of the allantois. *Development* **130**, 2681-2693.
Naiche, L. A., Harrelson, Z., Kelly, R. G. and Papaioannou, V. E. (2005). T-box genes in vertebrate development. *Annu. Rev. Genet.* **39**, 219-239.
Newman, P. J. (1999). Switched at birth: a new family for PECAM-1. *J. Clin. Invest.* **103**, 5-9.
Newman, P. J. and Newman, D. K. (2003). Signal transduction pathways mediated by PECAM-1: new roles for an old molecule in platelet and vascular cell biology. *Arterioscler. Thromb. Vasc. Biol.* **23**, 953-964.
Newman, P. J., Hillery, C. A., Albrecht, R., Parise, L. V., Berndt, M. C., Mazurov, A. V., Dunlop, L. C., Zhang, J. and Rittenhouse, S. E. (1992). Activation-dependent changes in human platelet PECAM-1: phosphorylation, cytoskeletal association, and surface membrane redistribution. *J. Cell Biol.* **119**, 239-246.
Papaioannou, V. E. (2001). T-box genes in development: from hydra to humans. *Int. Rev. Cytol.* **207**, 1-70.
Rashbass, P., Cooke, L. A., Herrmann, B. G. and Beddington, R. S. (1991). A cell autonomous function of Brachyury in T/T embryonic stem cell chimaeras. *Nature* **353**, 348-351.
Rennebeck, G., Lader, E., Fujimoto, A., Lei, E. P. and Artzt, K. (1998). Mouse Brachyury the Second (T2) is a gene next to classical T and a candidate gene for tct. *Genetics* **150**, 1125-1131.
Rennebeck, G. M., Lader, E., Chen, Q., Bohm, R. A., Cai, Z. S., Faust, C., Magnuson, T., Pease, L. R. and Artzt, K. (1995). Is there a Brachyury the Second? Analysis of a transgenic mutation involved in notochord maintenance in mice. *Dev. Biol.* **172**, 206-217.
Rivera-Perez, J. A. and Magnuson, T. (2005). Primitive streak formation in mice is preceded by localized activation of Brachyury and Wnt3. *Dev. Biol.* **288**, 363-371.
Schlaeger, T. M., Qin, Y., Fujiwara, Y., Magram, J. and Sato, T. N. (1995). Vascular endothelial cell lineage-specific promoter in transgenic mice. *Development* **121**, 1089-1098.
Schmidt, C., Wilson, V., Stott, D. and Beddington, R. S. (1997). T promoter activity in the absence of functional T protein during axis formation and elongation in the mouse. *Dev. Biol.* **189**, 161-173.
Schulte-Merker, S. and Smith, J. C. (1995). Mesoderm formation in response to Brachyury requires FGF signalling. *Curr. Biol.* **5**, 62-67.
Searle, A. G. (1966). Curtailed, a new dominant T-allele in the house mouse. *Genet. Res.* **7**, 86-95.
Shalaby, F., Rossant, J., Yamaguchi, T. P., Gertsenstein, M., Wu, X.-F., Breitman, M. L. and Schuh, A. C. (1995). Failure of blood-island formation and vasculogenesis in Flk-1 deficient mice. *Nature* **376**, 62-66.
Showell, C., Binder, O. and Conlon, F. L. (2004). T-box genes in early embryogenesis. *Dev. Dyn.* **229**, 201-218.
Smith, J. L., Gesteland, K. M. and Schoenwolf, G. C. (1994). Prospective fate map of the mouse primitive streak at 7.5 days of gestation. *Dev. Dyn.* **201**, 279-289.
Snell, G. B. and Stevens, L. C. (1966). Early embryology. In *Biology of the Laboratory Mouse* (ed. E. L. Green), pp. 205-245. New York: McGraw-Hill.
Stott, D., Kispert, A. and Herrmann, B. G. (1993). Rescue of the tail defect of Brachyury mice. *Genes Dev.* **7**, 197-203.
Tam, P. P. L. and Beddington, R. S. P. (1987). The formation of mesodermal tissues in the mouse embryo during gastrulation and early organogenesis. *Development* **99**, 109-126.
Wilkinson, D. G., Bhatt, S. and Herrmann, B. G. (1990). Expression pattern of the mouse T gene and its role in mesoderm formation. *Nature* **343**, 657-659.
Wilson, V., Rashbass, P. and Beddington, R. S. (1993). Chimeric analysis of T (Brachyury) gene function. *Development* **117**, 1321-1331.
Wilt, F. H. (1965). Erythropoiesis in the chick embryo: the role of endoderm. *Science* **147**, 1588-1590.
Winnier, G., Blessing, M., Labosky, P. A. and Hogan, B. L. M. (1995). Bone morphogenetic protein-4 is required for mesoderm formation and patterning in the mouse. *Genes Dev.* **9**, 2105-2116.
Wong, C. W., Wiedle, G., Ballestrem, C., Wehrle-Haller, B., Etteldorf, S., Bruckner, M., Engelhardt, B., Gisler, R. H. and Imhof, B. A. (2000). PECAM-1/CD31 trans-homophilic binding at the intercellular junctions is independent of its cytoplasmic domain; evidence for heterophilic interaction with integrin alphaVbeta3 in Cis. *Mol. Biol. Cell* **11**, 3109-3121.
Yamaguchi, T. P., Dumont, D. J., Conlon, R. A., Breitman, M. L. and Rossant, J. (1993). flk-1, an flt-related receptor tyrosine kinase, is an early marker for endothelial cell precursors. *Development* **118**, 488-498.
Yamaguchi, T. P., Takada, S., Yoshikawa, Y., Wu, N. and McMahon, A. P. (1999). T (Brachyury) is a direct target of Wnt3a during paraxial mesoderm specification. *Genes Dev.* **13**, 3185-3190.
Zavadskaia, N. and Kobozieff, N. (1930). Sur le facteur léthal accompagnant l'anurie et la brachyurie chez la souris. *C. R. Acad. Sci.* **191**, 352-355.
Zucker, R. M., Hunter, E. S. and Rogers, J. M. (1999). Apoptosis and morphology in mouse embryos by confocal laser scanning microscopy. *Methods* **18**, 473-480.